

Article

Cu-Based Catalysts with Enhanced Thermal Stability for Cyclohexyl Acetate Hydrogenation: Studies on Cu⁺ and Cu⁰ Sites at Different Reduction Temperatures

Xinyao Yu ¹, Mudi Xin ² , Hui Yuan ², Liang Gao ^{1,*} , Aiguo Zheng ², Enhui Xing ¹, Xiaoxin Zhang ¹, Chengxi Zhang ¹  and Baoning Zong ^{1,*}

¹ State Key Laboratory of Catalytic Materials and Reaction Engineering, Research Institute of Petroleum Processing Co., Ltd., SINOPEC, Beijing 100728, China

² State Key Laboratory of Molecular Refining, Research Institute of Petroleum Processing Co., Ltd., SINOPEC, Beijing 100728, China

* Correspondence: gaoliang.ripp@sinopec.com (L.G.); zongbn.ripp@sinopec.com (B.Z.); Tel.: +86-010-82368654 (L.G.); +86-010-82368011 (B.Z.)

Abstract: Cyclohexene esterification–hydrogenation for the efficient production of cyclohexanol will be commercialized for the first time. Cu/MgO/Al₂O₃ catalysts with layered double hydroxides as precursors were developed, and the effect of altering the reduction temperature on the catalytic activity was explored. Fresh and spent Cu/MgO/Al₂O₃ catalysts exhibited excellent catalytic performance after thermal treatment during the hydrogenation of cyclohexyl acetate to cyclohexanol. STEM images showed that the Cu particles grew slightly, without obvious aggregation. Based on the results of XAES and in situ FTIR of the adsorbed CO method, optimal performance (conversion rate of 99.59% with 98.94% selectivity) was achieved, which was attributed to the synergistic effect on the surface-active Cu⁰ and Cu⁺ sites with Cu⁰/(Cu⁰ + Cu⁺) of around 0.70, and the ratios could be maintained at temperatures of 513–553 K. The morphology of Cu/MgO/Al₂O₃ catalysts was well preserved during the hydrogenation of cyclohexyl acetate, indicating potential industrial applications. The well-dispersed Cu/MgO/Al₂O₃ catalyst with a stable microstructure possesses an adjustable valence state and thermal stability during the hydrogenation of cyclohexyl acetate, giving it industrial application prospects.

Keywords: ester hydrogenation; Cu-based catalysts; cyclohexyl acetate; cyclohexanol; activated copper species



Citation: Yu, X.; Xin, M.; Yuan, H.; Gao, L.; Zheng, A.; Xing, E.; Zhang, X.; Zhang, C.; Zong, B. Cu-Based Catalysts with Enhanced Thermal Stability for Cyclohexyl Acetate Hydrogenation: Studies on Cu⁺ and Cu⁰ Sites at Different Reduction Temperatures. *Catalysts* **2023**, *13*, 737. <https://doi.org/10.3390/catal13040737>

Academic Editors: Maria Luisa Di Gioia, Luisa Margarida Martins and Isidro M. Pastor

Received: 10 March 2023

Revised: 5 April 2023

Accepted: 10 April 2023

Published: 13 April 2023



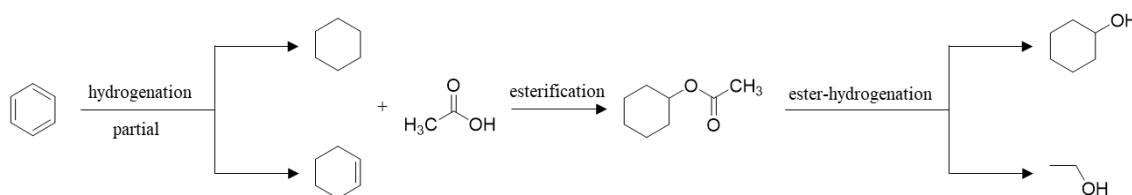
Copyright: © 2023 by the authors. Licensee MDPI, Basel, Switzerland. This article is an open access article distributed under the terms and conditions of the Creative Commons Attribution (CC BY) license (<https://creativecommons.org/licenses/by/4.0/>).

1. Introduction

Cyclohexyl acetate (CHA) is a key intermediate that can be used to produce caprolactam and adipic acid. The organic chemical raw materials cyclohexanol (CHOL) and cyclohexanone are used to make ϵ -caprolactam and adipic acid [1]. The market value of ϵ -caprolactam is expected to reach 18.6 billion USD by 2023. As a result, the enormous demand for CHOL and cyclohexanone has drawn increasing attention from academics and industry.

Three traditionally commercial CHOL production processes have been applied to date: cyclohexane oxidation [2], cyclohexene hydration [3–5], and phenol hydrogenation [6]. The cyclohexane oxidation process must be operated at a low conversion rate, which results in considerable energy consumption during the separation of the product, by-product, and unreacted cyclohexane. The process of hydrogenation from phenol to CHOL is relatively complicated, which produces poisons, and is prone to the corrosion of equipment. The conversion rate is relatively low, separation energy consumption is high, and equipment investment is significant. These are the drawbacks of the cyclohexene hydration technique. Therefore, developing a novel method for efficiently synthesizing CHOL is imperative.

Zong et al. proposed a novel cyclohexene-esterification-hydrogenation route to produce CHOL (Scheme 1) [7]. In the novel route, the acetate is subsequently hydrogenated to obtain ethanol and CHOL, and the CHOL is dehydrogenated to become cyclohexanone. This novel cyclohexene esterification-hydrogenation route provides better atom economy and yields than the three above-mentioned procedures, especially cyclohexene esterification and CHA hydrogenation, which have yields higher than 99% and 99.5%, respectively. This novel route, which has been elucidated in detail in previous work [7], has been demonstrated on long-term, pilot-scale units and will be commercialized at a scale of 400,000 tons per year in SINOPEC Co., Ltd., in 2023. Due to their remarkable selectivity in C-O hydrogenation, copper-based catalysts have received a great deal of attention [8] and are widely used in the catalytic hydrogenation of carbonyl-containing compounds such as dimethyl oxalate [9–12] and other cyclic compound derivatives [13–15].



Scheme 1. The novel cyclohexene-esterification-hydrogenation process to produce CHOL, starting from benzene.

To the best of our knowledge, the sintering and coalescence of copper nanoparticles are among the most common causes of deactivation due to the low Hüttig temperature (surface mobility of atoms) and high Tamman temperature (bulk mobility) for copper at just 407 and 678 K, respectively [16]. Copper-based catalysts suffer from poor durability and thermal stability as a result of the aggregation of copper particles, the loss of active copper surface, and the valence transition of cupreous species under reaction conditions. The inhibition of copper migrations and aggregations is critical to enhancing the thermal stability of Cu-based hydrogenation catalysts. The majority of researchers reached a consensus regarding the inhibition of metallic copper's migration in the design of many strategies to improve the stability of the catalyst. Sun's group established [17–19] a type of heterogeneous copper catalysts prepared via sputtering and flame-spray pyrolysis methods, characterized by copper stability at ultra-high temperatures of up to 1073 K, and proposed using them in hydrogenation, oxidation, reforming reactions, and other forms of high-temperature processing. Additionally, the active site of the Cu species is also crucial to the catalytic performance of a Cu-based catalyst. Among the various views on active sites [20–27], synergism between Cu^0 and Cu^+ is commonly accepted [22,27]. According to the proposed synergism, in different reactions, the Cu^0/Cu^+ ratio should correspond to the catalytic activity, although different studies have reached opposite conclusions [28–31]. In brief, Cu^0 improves H_2 dissociation, whereas Cu^+ functions as a Lewis acid site to adsorb and activate carbonyl [32,33].

In our previous work [7], $\text{Cu}/\text{ZnO}/\text{SiO}_2$ and $\text{Cu}/\text{ZnO}/\text{Al}_2\text{O}_3$ catalysts were developed for the hydrogenation of CHA at a pilot scale, but the variables influencing the conversion of CHA and its selectivity to CHOL were not thoroughly investigated. Li's group also conducted a similar work using the same ester hydrogenation process, and the reaction occurred in an autoclave, in which the reaction temperature reached 553 K without deactivation [34]. Meanwhile, this process faces the unmentioned problem of high-temperature inactivation. Herein, $\text{Cu}/\text{MgO}/\text{Al}_2\text{O}_3$ catalysts with a layered double hydroxide (LDH) precursor were prepared by the co-precipitation method to constrain the Cu species from migration and aggregation [35,36]. The commercial $\text{Cu}/\text{ZnO}/\text{Al}_2\text{O}_3$ catalyst and an amorphous $\text{Cu}/\text{MgO}/\text{Al}_2\text{O}_3$ catalyst were also compared after thermal treatment. The regular micro-structures were preserved to favor better thermal stability due to the spatial confinement of metallic copper atoms achieved by enhancing the interactions between

oxide lattices and the copper species. Furthermore, we revealed an activation strategy that could be induced to manipulate the surface amounts and proportions of Cu^0 and Cu^+ by improving the reduction temperatures from 453 to 593 K. The ratio of $\text{Cu}^0/(\text{Cu}^0 + \text{Cu}^+)$ was characterized by XPS, using the in situ FTIR of CO adsorption method.

2. Results and Discussion

2.1. Different Cu-Based Catalysts

The XRD patterns of the calcined CMA-L, CMA-A, and CZA-C catalysts are shown in Figure 1A. Figure 1A displays the XRD patterns of the precursor CuMgAl-LDH. The precursor showed clear peaks at 12.3° (003), 24.4° (006), 34.7° (012), 39.0° (015), 46.4° (018), and 60.8° (110), which correspond to magnesium-aluminum hydroxide hydrate (JCPDS35-0965) [35]. Compared with the standard LDH structure, all of the diffraction peaks were shifted slightly, which was attributed to the Jahn–Teller effect of Cu^{2+} , which led to the distortion of its octahedral lattice structure, accordingly increasing the disorder of the crystal form [37]. According to the XRD patterns of the precursor, the interplanar spacing and lattice parameters were calculated: the interplanar spacing— $d_{003} = 0.721$ nm, $d_{006} = 0.364$ nm, and $d_{110} = 0.152$ nm; and the lattice parameters— $a = 0.305$ and $c = 2.163$. This is consistent with the configuration of hydrotalcite (3R), and the diffraction peaks validated the standard pattern of Mg–Al hydrotalcite. The diffraction peaks at 32.5° (110), 35.5° (11-1), 38.7° (111), 48.7° (20-2), and 61.5° (11-3) were attributed to the crystal faces of CuO (JCPDS 48011548). Calcined CMA-L showed sharp diffraction peaks in CuO, which was obtained by the well-ordered LDH phase precursor. The amorphous calcined samples of CMA-A and CZA-C showed a low degree of crystallinity and weak diffraction peaks in CuO, implying that the micro-structure was conducive to improving the crystallinity of CuO.

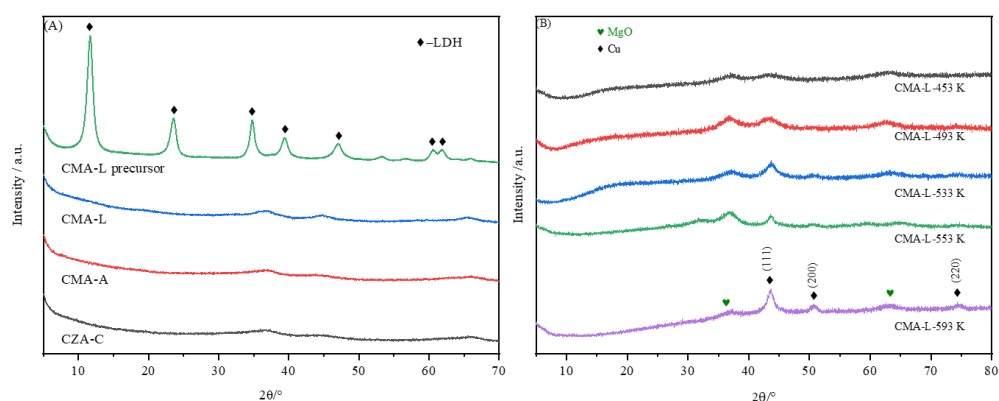


Figure 1. XRD patterns of the precursors CMA-L-LDH, and calcined samples CMA-L, CMA-A, and CZA-C (A). The reduced samples of CMA-L (B).

After reduction treatment at 453–593 K, the CMA-L samples were also characterized by XRD. The crystal planes of Cu (111), (200), and (220) were attributed to the diffraction peaks at 2θ of 43.3° , 50.4° , and 74.1° . (JCPDS 85-1326). The (111), (200), and (220) crystal planes of MgO (JCPDS 87-0653) were responsible for the diffraction peaks at 2θ of 37.0° , 43.0° , and 62.5° , respectively. Regarding the CMA-L catalysts, the characteristic peaks of Cu became stronger as the reduction temperature increased, which illustrated that the particle size of Cu increased. The formation of an LDH precursor implied that Cu particles were strongly anchored by the well-ordered structure at a suitable reduction temperature.

Table 1 shows the chemical compositions and textural properties of the calcined CMA-L, CMA-A, and CZA-C samples. The actual contents of CuO, MgO, ZnO, and Al_2O_3 in Cu-based catalysts were measured by XRF analysis.

Table 1. Physicochemical properties of the calcined samples of CMA-L, CMA-A, and CZA-C.

Catalysts	Elemental Compositions ¹ (wt %)			S_{BET} ² (m ² /g)	V_{pore} ² (cm ³ /g)	D_{pore} ² (nm)	D_{M} ³ (%)
	CuO	MgO or ZnO	Al ₂ O ₃				
CMA-L	51.0	20.6 (MgO)	26.6	154.8	0.55	14.2	40
CMA-A	34.3	17.2 (MgO)	45.6	133.2	0.46	14.0	34
CZA-C	27.5	39.0 (ZnO)	31.4	144.7	0.25	6.9	38

¹ Elemental compositions of CuO, MgO, ZnO, and Al₂O₃ measured by XRF analysis. ² BET surface area (S_{BET}), pore volume (V_{pore}), and pore size (D_{pore}) were measured by N₂ adsorption and desorption. ³ D_{M} represents the surface copper dispersion and measured by H₂-N₂O titration experiments.

The porous characteristics and the as-calcined catalysts were identified using nitrogen sorption, as shown in Table 1. CMA-L had the largest surface area, pore volume, and pore size, which was due to the regular micro-structure. The BET surface area did not change noticeably when Zn or Mg species were loaded. However, the pore volume and pore size of CMA-L and CMA-A decreased compared with CZA-C. Evidently, the presence of Mg might have noteworthy impacts on the pore properties. The dispersion of copper species was further investigated with H₂-N₂O titration experiments. In contrast, the CMA-L showed the greatest dispersion of metallic copper species (Table 1), a result of the LDH phase precursor's well-ordered structure and large specific surface (the largest).

Some related characterization methods were used to further understand the Cu-based catalysts. H₂-TPR experiments on as-calcined samples were carried out to study the reducibility of Cu species and the interaction of Cu and other metal species. Figure 2 displays the H₂-TPR curves of the calcined samples. The distribution of the reduction peaks shows a clear contrast between the catalysts. As illustrated in Figure 2, the reduction from Cu²⁺ species to Cu⁺ and Cu⁰ species corresponded to a decrease in overall hydrogen consumption. The reduction peak distribution demonstrated a clear difference between the catalysts. The presence of magnesium in the catalysts CMA-L and CZA-C caused the major reduction temperature to shift to a lower-temperature area. We can conclude that the interaction between Cu species and Mg may promote the reducibility of Cu species. In the case of CMA-A, the peak at high temperature (506.3 K) was attributed to the reduction in Cu²⁺ species in the form of larger-sized composite metal oxides or to strong interactions between CuO and other metal oxides, whereas the small shoulder at a low temperature (458.6 K) was attributed to the reduction in smaller, isolated, highly dispersed CuO [38]. Regarding CMA-L and CZA-C, which originated from the presence of highly dispersed copper species, the Cu²⁺ species were reduced more readily at 452.0 and 511.8 K, respectively (Table 1). Due to the layer framework of the LDH precursor structure, CMA-L had the lowest hydrogen consumption peak, centered at 452.0 K, indicating the well dispersed copper species present in the CuO. The highest hydrogen consumption peak of CZA-C was attributed to the reduction in the largest crystalline CuO. As a result, the interaction of copper species with the carrier and the dispersion of copper species on the carrier's surface had a significant impact on the reduction behaviors of the Cu-based catalysts.

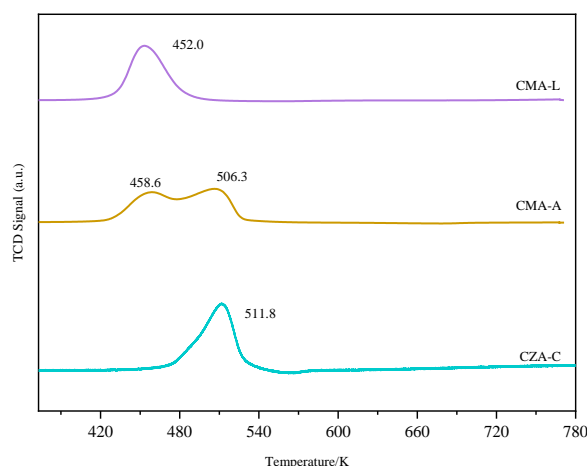
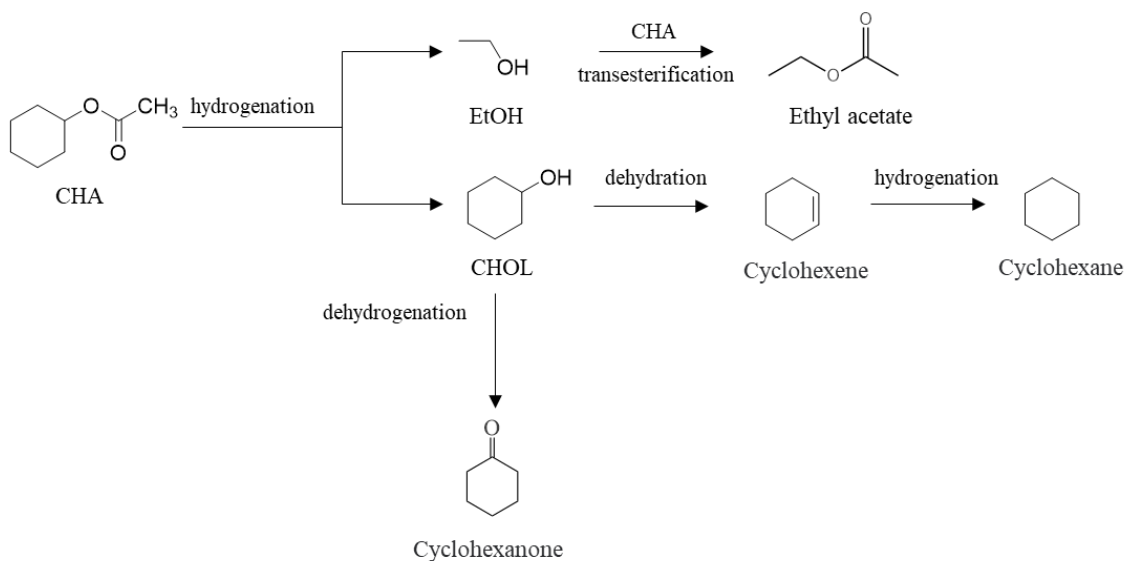


Figure 2. H₂-TPR curves in CMA-L, CMA-A, and CZA-C after calcination.

2.2. Thermal Stability

The hydrogenation of CHA over CMA-L, CMA-A, and CZA-C was carried out. The products were reduced in situ on the fixed-bed reactor, as described in Section 2.3. Byproducts included ethyl acetate, cyclohexene, cyclohexane, and cyclohexanone (Scheme 2).



Scheme 2. The reaction pathway for selective hydrogenation from CHA to CHOL.

To investigate the Cu-based catalysts, the influences of WHSV, hydrogen pressure, and reaction temperature were explored further using CMA-L as a representative. As shown in Figure 3A,B, the reaction temperature was optimized in the range of 473–533 K. Notably, CMA-L derived from LDH displayed stable CHA conversion rate and CHOL selectivity above 90%, making it significantly superior to amorphous CMA-A and commercial CZA-C. As for CZA-C, the conversion rate increased from 94.7% to 99.4% in the temperature range 473–533 K, followed by a slight decrease from 98.3% to 90.1% (within 553–573 K). CMA-A showed a large variation with increasing reaction temperature—rising from 70.3% (at 473 K) to 90.9% (at 513 K) and then decreasing (within 533–573 K). However, the selectivity of the three catalysts stayed high (above 94%) as the reaction temperature ranged from approximately 473 to 553 K. A slight increase in selectivity to CHOL was observed from approximately 553 to 573 K because of the increase in the content of both cyclohexene and cyclohexane.

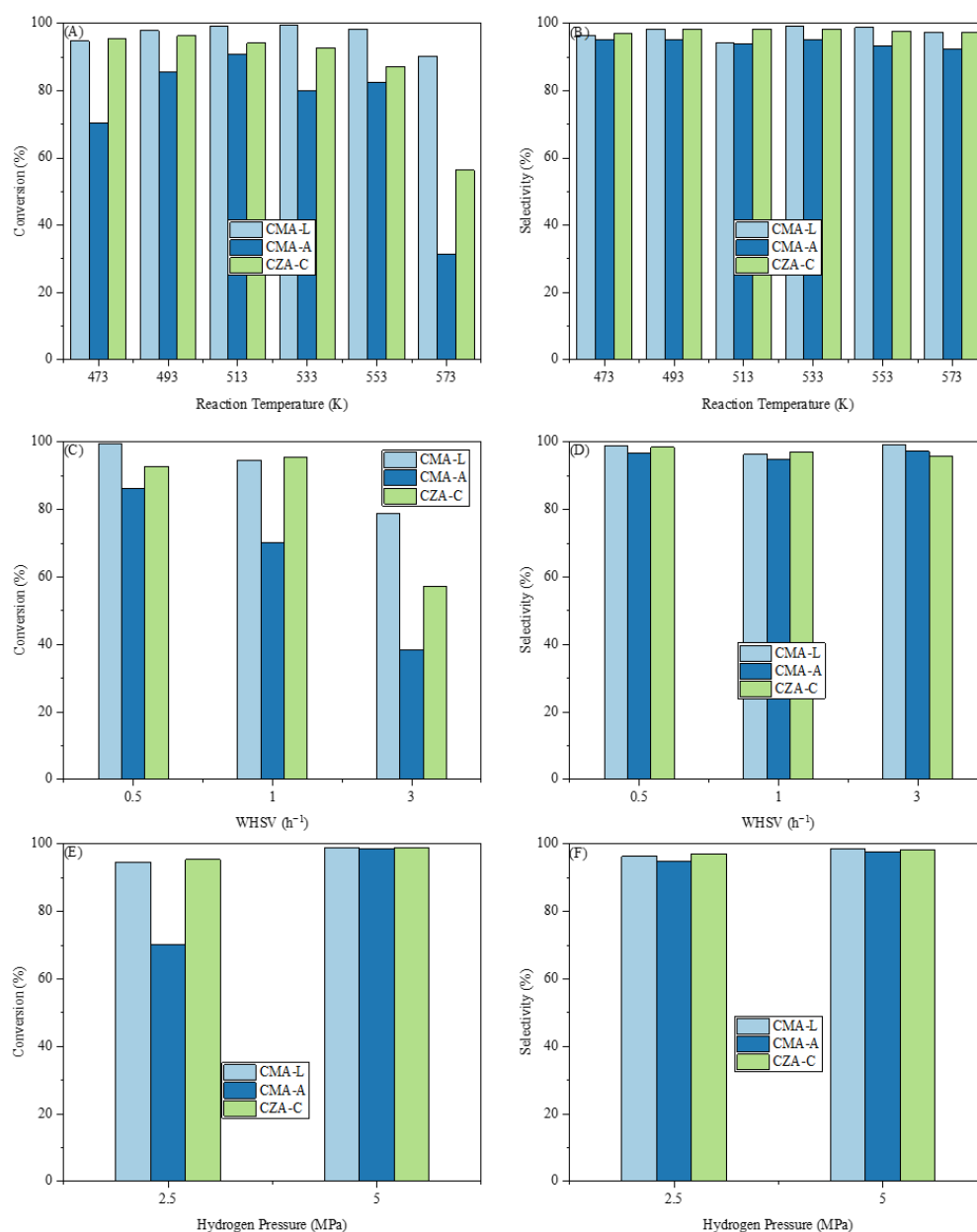


Figure 3. The effects of reaction parameters on the hydrogenation of CHA over Cu-based catalysts: conversion rate (A) and selectivity (B) at different reaction temperatures, obtained after reduction at 523 K, H₂ pressure: 2.5 MPa, H₂/CHA molar ratio = 20:1, WHSV = 1.0 h⁻¹; conversion rate (C) and selectivity (D) at different WHSVs, after reduction at 523 K, and the reaction at 473 K, H₂ pressure: 2.5 MPa, H₂/CHA molar ratio = 20:1, conversion rate (E) and selectivity (F) at hydrogen pressures of 2.5 MPa and 5.0 MPa, after reduction at 523 K, and the reaction at 473 K, H₂/CHA molar ratio = 20:1, WHSV = 1.0 h⁻¹.

Subsequently, the influence of WHSV was also investigated. Figure 3C,D shows that the CMA-L achieved nearly 100% CHA conversion rate and 98.8% CHOL selectivity under the optimal conditions (WHSV = 0.5 h⁻¹), outperforming other catalysts. As WHSV increased, the conversion rate of CHA gradually decreased while the selectivity for CHOL remained essentially the same.

Furthermore, the effect of hydrogen pressure was investigated at 2.5 and 5.0 MPa (Figure 3E,F); a significant improvement in the CHA conversion rate of CMA-A was observed, from 70.3% to 98.7%. As hydrogen pressure increased, the CHA conversion rates

of CMA-L and CZA-C were also marginally improved. The selectivity to CHOL changed, although not very obviously, as the hydrogen pressure increased.

Furthermore, thermal stability is an exceedingly vital indicator of a heterogeneous catalyst. In order to further study intrinsic thermal stability, the space-time yields (STYs) of CHOL for fresh and spent catalysts were calculated and are presented in Table 2. Fresh catalyst was evaluated at reaction temperature (473 K), and then after a 24 h thermal treatment at 593 K, the STY of the spent catalyst was achieved after the reaction temperature was adjusted to 473 K. After thermal treatment, the catalytic performance of CHA hydrogenation over CMA-L showed a slight decrease (STY from 0.91 to 0.82) compared to CMA-A and CZA-C. After thermal treatment, CMA-A was clearly inactivated; STY dropped from 0.67 to 0.28. STY also showed an obvious decrease for the CMA-C catalyst (from 0.92 to 0.50). This suggested that the thermal stability of CMA-L with a micro-structure was superior to the stability of amorphous CMA-A and CZA-C.

Table 2. STY of fresh and spent catalysts (reaction condition: 473 K, H₂ pressure: 2.5 MPa, H₂/CHA molar ratio = 20:1, WHSV = 1.0 h⁻¹).

Catalyst	STY	
	Fresh	Spent
CMA-L	0.91	0.82
CMA-A	0.67	0.28
CZA-C	0.92	0.50

In order to verify the enhanced thermal stability of CMA-L, the fresh and spent catalysts were characterized by STEM mapping. Figure 4 shows the STEM images and EDX maps of Cu from the copper-based catalysts. Figure 4a is a scanning TEM (STEM) image of a typical structure of nanoflakes, on which an elemental mapping analysis was performed. The EDX elemental maps revealed that the compositional distributions of the Cu in the CMA-L, whether before or after reaction, were uniform, suggesting that the microstructures could be retained to prevent the aggregation of Cu species. A clear difference was observed in HAADF-STEM images (Figure 4c,d) of the amorphous catalyst CZA-C, further confirming the Cu was aggregated into the bulk phase, which was consistent with the results of catalyst deactivation after evaluation. Similarly, CMA-A (Figure 4e,f), as a contrast agent, also showed obvious aggregation of Cu particles after the reaction.

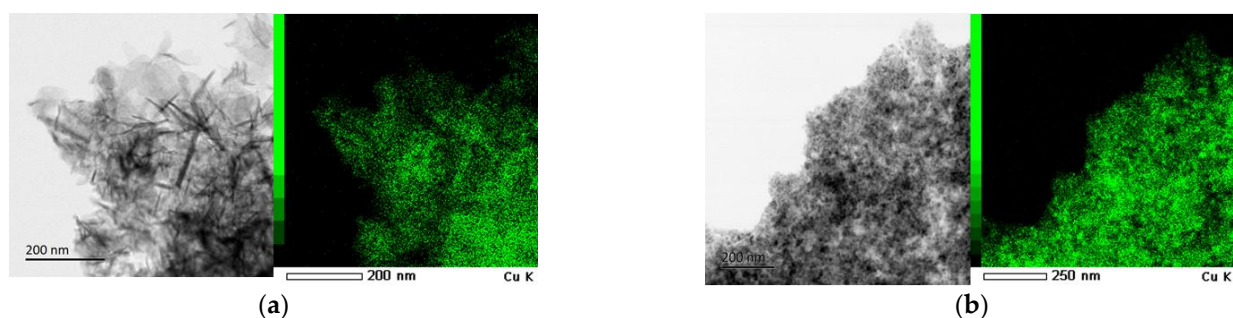


Figure 4. Cont.

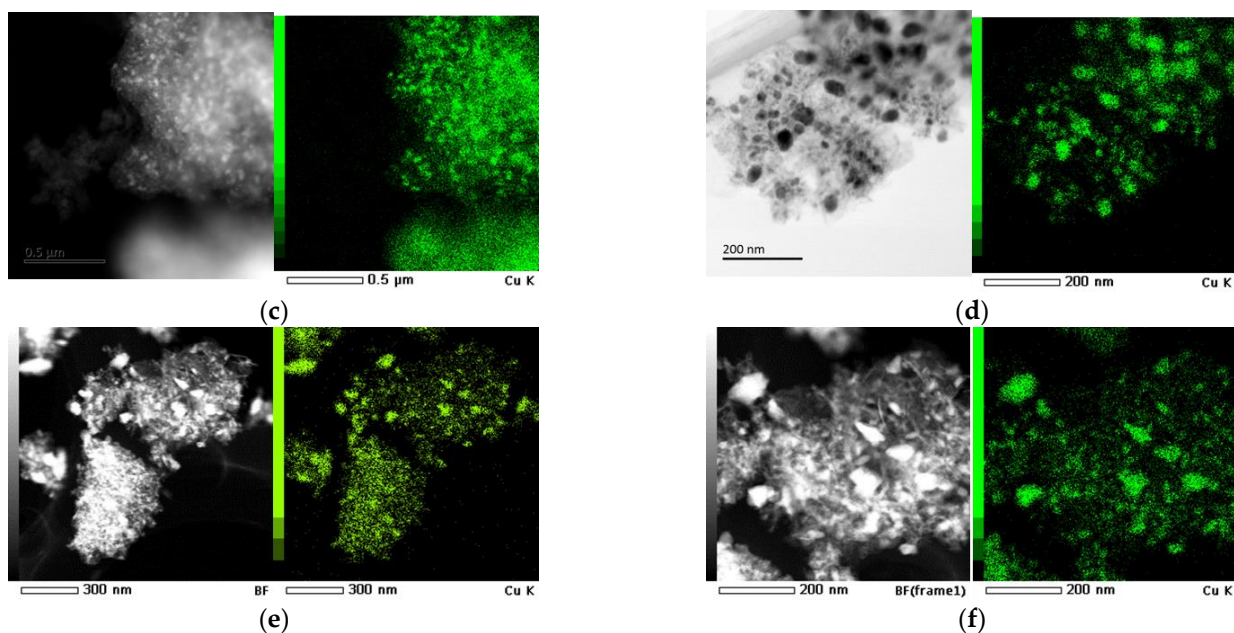


Figure 4. STEM image and EDX maps of Cu of the fresh CMA-L (a), spent CMA-L (b), fresh CZA-C (c), spent CZA-C (d), fresh CMA-A (e), spent CMA-A (f).

Ensuring a catalyst's long-term stability is critical for practical industry applications, to guarantee a long life for it. Figure 5 presents the catalytic hydrogenation performance as a function of the duration on a stream over CMA-L at the optimal reaction conditions (473 K, H_2 pressure: 2.5 MPa, H_2/CHA molar ratio = 20:1, WHSV = 0.5 h^{-1}). It was noted that CMA-L exhibited high stability (conversion rate of 99.59% with 98.94% selectivity) for the hydrogenation of CHA for up to 500 h, and no decrease in either the conversion rate of CHA or the selectivity to CHOL could be observed. Excellent catalytic performance and better stability were demonstrated by the designed CMA-L with an appropriate $Cu^0/(Cu^0 + Cu^+)$ ratio and microstructure.

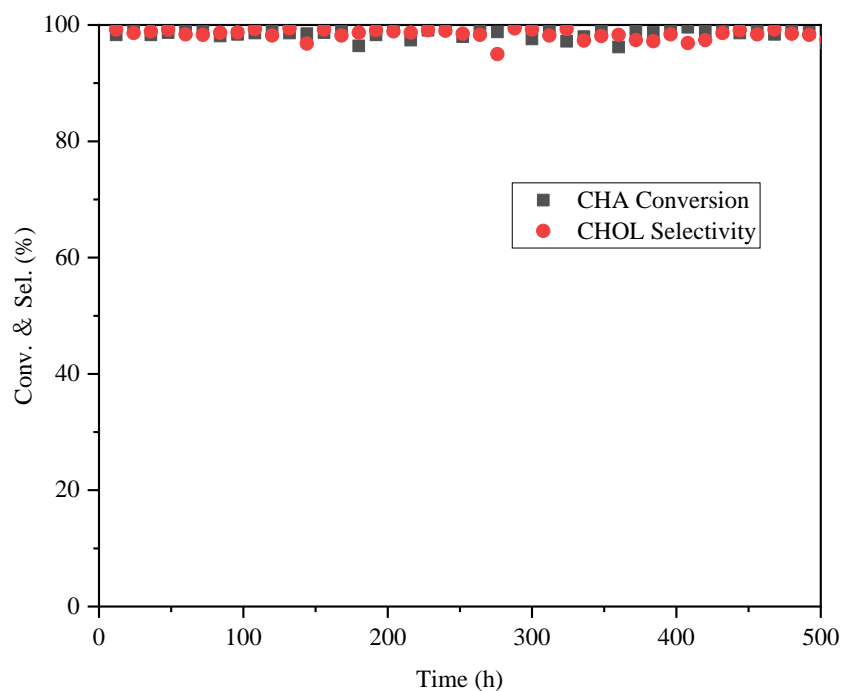


Figure 5. Long-term performance of CHA hydrogenation over CMA-L. Reaction conditions: 473 K, H_2 pressure: 2.5 MPa, H_2/CHA molar ratio = 20:1, WHSV = 0.5 h^{-1} .

2.3. Induced Activation Process

To understand the thermal stability of CMA-L, we evaluated the reaction performance of CMA-L at different reduction temperatures. As listed in Table 3, the CHA conversion, CHOL selectivity, and TOF were measured under a high WHSV. CMA-L with an LDH precursor significantly maintained the highest activity and 76–79% conversion, together with 98–99% selectivity to CHOL. The TOF was maintained at 3.2–3.3 when the reduction temperature was in the range of 513–533 K. The TOF, conversion rate, and selectivity all dropped slightly as the reduction temperature was increased.

Table 3. Results of CHA hydrogenation performance over CMA-L.

Catalyst	Reduced Temperature/K	TOF/h ⁻¹	Conversion/%	Selectivity/%
CMA-L	453	2.4	56.8	98.6
	513	3.3	78.7	98.0
	533	3.3	78.9	99.1
	553	3.2	76.4	98.8
	593	2.3	56.4	97.9
CZA-C	533	2.6	57.2	95.7
CMA-A	533	2.5	38.4	97.2

Reaction condition: 483 K, H₂ pressure: 2.5 MPa, H₂/CHA molar ratio = 20:1, WHSV = 3 h⁻¹.

It is widely recognized that the surface chemical states of Cu-based catalysts, particularly the ratio of Cu⁰ to Cu⁺, have an impact on their catalytic performances [39]. We demonstrated an induced activation strategy for controlling the composition of Cu⁰ and Cu⁺ to manipulate the catalyst-surface-reconstruction process. XPS was performed on CMA-L at various reduction temperatures (453–593 K) to investigate the surface chemical states of Cu species. Before the XPS test, the catalyst was reduced to H₂ via tube furnace, passivated, and sealed with an ethanol solution. As shown in Figure 6A, the spectra of CMA-L samples displayed Cu 2p_{3/2} (about 932.5 eV), Cu 2p_{1/2} peaks (about 952.2 eV), and satellite peaks (940–945 and 960–965 eV) (Figure 6A). The satellite peak depicts the characteristic peaks in Cu²⁺ species on the surface of the reduced CMA-L sample [40–42]. The satellite area decreased in the lower temperature range of 453–593 K, which confirmed that the content of Cu²⁺ was also gradually decreasing. Cu LMM Auger electron spectra were used in Figure 6B due to the proximity of the Cu 2p binding energies for Cu⁺ and Cu⁰. On the Cu LMM spectra, the kinetic energies of Cu²⁺, Cu⁺, and Cu⁰ were, respectively, 913, 916, and 918.5 eV [43]. The ratio of Cu⁰/(Cu⁰ + Cu⁺) was calculated using the Cu LMM spectra in Table 4 in order to more clearly survey the variation in Cu species' states.

Table 4. Cu LMM results of CMA-L catalysts after reduction.

Reduction Temperature/K	Kinetic Energy (eV)			Ratio/%			Cu ⁰ / (Cu ⁰ + Cu ⁺)
	Cu ²⁺	Cu ⁰	Cu ⁺	Cu ²⁺	Cu ⁰	Cu ⁺	
453	916.2	918.5	913.0	47.0	32.2	20.8	0.61
493	916.2	918.5	913.1	41.0	40.0	19.0	0.68
533	916.2	918.5	913.4	40.5	40.4	19.1	0.68
553	916.2	918.5	913.0	37.3	43.8	19.0	0.70
593	916.2	918.5	913.5	27.3	55.7	17.1	0.77

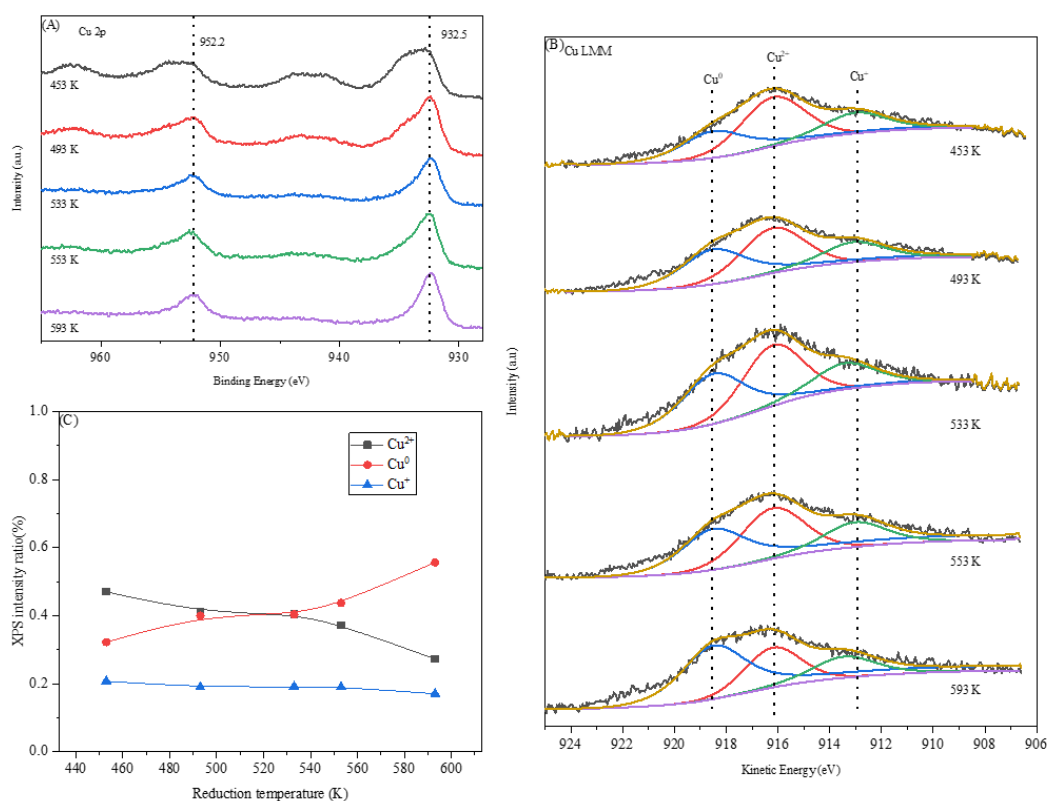


Figure 6. Samples of CMA-L after reduction at 453–593 K: XPS spectra of Cu 2p (A), corresponding spectra of Cu LMM (B), and ratios of copper species (C).

According to Figure 6C, increasing the reduction temperature improves reduction, and this is enhanced by the transformation from Cu²⁺ to Cu⁰. The content of Cu⁺ ions was maintained at approximately 20% over a wide temperature range of 453–593 K, which is distinct from Hu’s results [41] regarding the intensity ratio of Cu⁺ and Cu²⁺ to Cu⁰. Hu’s research on Cu/Al₂O₃ revealed that the quantity of Cu²⁺ rapidly decreased while that of Cu⁰ continuously increased. A similar pattern was found in copper phyllosilicate nanotubes for dimethyl oxalate hydrogenation [44] and in other research [27,42]. The aggregation or partial coating of Cu was indicated by a linear decline in Cu content. It is worth noting that our results could be explained by the fact that the reduction procedure was a cascade reaction, with Cu⁺ acting as an intermediate and remaining at a low proportion of the total. The percentages representing Cu⁰ and Cu²⁺ remained at relatively stable values throughout the temperature range from 493 to 553 K, and the molar ratios of Cu⁰/(Cu⁰ + Cu⁺) that were calculated were approximately 0.70. The results also indicated that the reduction in the well-dispersed CuO in CMA-L was hindered either by spatial confinement or the strong interaction between Cu species in the oxide lattices at the medium range of temperatures. Cu⁰/(Cu⁰ + Cu⁺) showed no change at temperatures ranging from 493 to 553 K. This improved significantly until reduction temperatures of 593 K or higher were reached. The synergy of Cu⁰ and Cu⁺ is critical in the ester hydrogenation reactions. H₂ could be adsorbed and dissociated on the Cu⁰, and the Lewis acid sites or electrophilic sites on the Cu⁺ serve to trigger the long-pair electrons on the carbonyl groups [32,33].

The in-depth reduction was further characterized by an in situ FTIR study of the CO adsorbed in this work with the aim of validating the Cu 2p and Auger signal of Cu LMM results. CO is frequently utilized to investigate the characteristics of Cu-containing catalysts due to its comparatively simple molecular structure and outstanding coordination capabilities with Cu species. Researchers were able to determine the metal’s active center on the catalyst and the difference in the activity in the surrounding electronic environment by measuring and comparing the infrared spectra of adsorbed CO. The catalytic reaction mechanism could be determined by measuring and comparing the infrared spectra of

adsorbed CO. As elucidated in previous work, the 2000–2200 cm^{-1} FTIR absorption bands of CO adsorption are commonly used to discriminate different chemical states of Cu [45]. The interaction of the CuO, Cu₂O, or Cu⁰ sites with linear or bridge-bonded CO has been linked to bands in the first region [45]. The relative quantities of Cu species can also be quantified using CO adsorption on distinct Cu species.

Figure 7 showed the band of CO during the in situ reduction in pre-treatment CMA-L under low-temperature, liquid-nitrogen conditions. During the 10% H₂/N₂ reduction process at temperatures ranging from 454 to 593 K, the adsorbed CO quantities under various conditions were fairly believable, as the operation took place on the same sample flake as that mentioned above in Section 3.2. The deconvolution area of the CO adsorption peak was taken as a function of reduction temperature. A volcanic-type curve appeared, implying that the quantity of CO absorption increases and then drops as the reduction temperature increases.

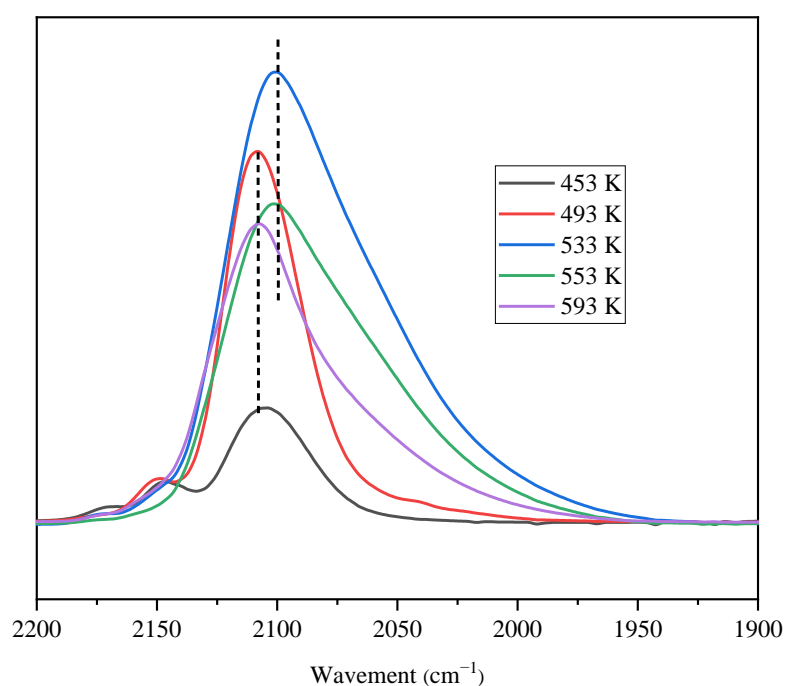


Figure 7. In situ FTIR of the adsorbed CO method using CMA-L catalysts reduced at 454–593 K.

According to Vannice et al.'s work [45], partial peaking fitting was carried out. Table 5 displays the relative proportions of Cu species with various valences and the calculated molar ratios of Cu⁰/(Cu⁰ + Cu⁺). According to Table 5, the proportions of Cu⁰ and Cu⁺ increased with reduction temperature, and the Cu⁰/(Cu⁰ + Cu⁺) ratios rose to around 0.70 between 453 and 553 K, and then fell to 0.60 at 593 K. Cu⁺ could be assigned a band of 2107–2111 cm^{-1} , and Cu⁰ could be assigned a band of 2080–2094 cm^{-1} . The frequencies of Cu⁰ were attributed to the different Cu facets [46] or Coppers' different surface surroundings [46].

Table 5. CMA-L in situ FTIR of the adsorbed CO method's peak fitting results.

Catalysts with Reduction Temperature/K	CO Frequency/cm ⁻¹		Ratio/%		Cu ⁰ /(Cu ⁰ + Cu ⁺)
	Cu ⁺	Cu ⁰	Cu ⁺	Cu ⁰	
453	2108	2093	47.64	33.74	0.41
493	2111	2094	48.86	44.84	0.48
533	2107	2080	28.21	71.79	0.72
553	2108	2080	32.01	67.99	0.68
593	2110	2084	40.30	59.70	0.60

The Cu⁰/(Cu⁰ + Cu⁺) curves and trends obtained by the in situ FTIR of the adsorbed CO method differed significantly from those of Cu LMM (Table 6). A data comparison revealed that the variation in the Cu⁰/(Cu⁰ + Cu⁺) ratio might be more reasonable. Firstly, the ratios being approximately 0.70 at reduction temperatures of 533 K and 553 K, observed by two different characterizations, suggests that the ratios are reliable. Secondly, regarding the ratios of reduction temperatures at 453 and 493 K, it was proposed that the results of in situ FTIR of adsorbed CO were reliable for determining the bulk contents of Cu²⁺, Cu⁺, and Cu⁰ from the information acquired from transmission infrared spectra, and the XPS measurements were associated with the several superficial layers of the catalysts. The copper species in the bulk phase were hydrogenated to a lower degree than those on the surface at relatively lower temperatures of 453 and 493 K. As a result of the enrichment of Cu⁰ and Cu⁺, the results of Cu⁰/(Cu⁰ + Cu⁺) are relatively high. The Cu LMM results are suggested to be reliable at higher temperatures, with a Cu⁰/(Cu⁰ + Cu⁺) ratio of 0.79. The higher reduction temperature, in our opinion, caused the Cu species inside the catalysts to reduce to a greater degree than the superficial ones. Simultaneously, higher reduction temperatures promote Cu⁰ aggregation, reducing the exposure of Cu⁰ species sites. As a result, the intensity of the in situ FTIR of adsorbed CO measurements will be lower than the exact value, even though the Cu⁰ proportion increases at elevated temperatures.

Table 6. Determination of Cu⁰/(Cu⁰ + Cu⁺) ratio by various CMA-L characterization methods.

Catalysts with Reduction Temperature/K	Cu LMM	In Situ FTIR of Adsorbed CO Method
453	0.61	0.41
493	0.68	0.48
533	0.68	0.72
553	0.70	0.68
593	0.77	0.60

Several studies have noted that a synergistic interaction between Cu⁺ and Cu⁰ is essential for ester hydrogenation, such as from dimethyl oxalate to ethylene glycol in Cu/SiO₂ catalytic systems. However, discussions about our system during the hydrogenation of CHA are absent. The ratio of Cu⁰/(Cu⁰ + Cu⁺) can remain at ~0.70 during the activation process (reduction temperatures of 533 and 553 K), as opposed to the linear relationship, as in previous works [41,42,44]. We discovered that the greatest TOF of the catalyst was around 3.3 at the reduction temperature of 513 to 553 K when combined with the evaluation data in Table 3. The surface Cu state of the sample and the catalyst's catalytic efficiency have a strong correlation. When the ratio of Cu⁰ is about 0.70, the catalytic activity also reaches its peak. The proportion of Cu⁰/(Cu⁰ + Cu⁺) needs to be in an appropriate range for the ester hydrogenation reaction to exhibit the superior catalytic effect.

The results above substantiate that the synergistic catalysis of Cu⁰ and Cu⁺ plays a vital role in the CHA hydrogenation reaction. The hydrogenation from CHA to CHOL on CMA-L can be explained by a potential reaction mechanism. H₂ can be adsorbed and dissociated by Cu⁰ on the catalyst's surface, and the carbonyl group's oxygen atoms can

be adsorbed and polarized by Cu^+ . [28–31]. The ratio of $\text{Cu}^0/(\text{Cu}^0 + \text{Cu}^+)$ can remain at -0.70 , which may be the reason for the superior thermal stability of CMA-L.

3. Materials and Methods

3.1. Catalyst Preparation

$\text{Cu}/\text{MgO}/\text{Al}_2\text{O}_3$ catalysts (CMA-L) were prepared by a typical co-precipitation reported in the literature [43]. The method can be briefly described as follows: Solution A: $\text{Cu}(\text{NO}_3)_2 \cdot 3\text{H}_2\text{O}$, $\text{Mg}(\text{NO}_3)_2 \cdot 6\text{H}_2\text{O}$, and $\text{Al}(\text{NO}_3)_3 \cdot 9\text{H}_2\text{O}$ with the $\text{Cu}^{2+}/\text{Mg}^{2+}/\text{Al}^{3+}$ molar ratio of 3:4:3 were dissolved in 200 mL of deionized water. Solution B: NaOH and Na_2CO_3 were dissolved in 350 mL of deionized water. In solution A, the concentrations of the base and the metal ions were correlated as: $[\text{CO}_3^{2-}] = 2[\text{Al}^{3+}]$, $[\text{OH}^-] = 1.6([\text{M}^{2+}] + [\text{Al}^{3+}])$. Solutions A and B were added together drip by drip, at the same time, maintaining a pH of 10.5. The resulting blue suspension was aged at 313 K for 8 h, washed several times with deionized water until the pH of the filtrate reached 7.0, and finally dried at 393 K for 12 h to obtain the precursor CuMgAl-LDH . The CuMgAl-LDH was pelletized, crushed, and sieved to 20–40 mesh after being calcined in static air at 673 K for 4 h.

In contrast, $\text{Cu}/\text{MgO}/\text{Al}_2\text{O}_3$ (CMA-A) catalysts were also prepared using the same method. The preparation method was as follows: Solution A: $\text{Cu}(\text{NO}_3)_2 \cdot 3\text{H}_2\text{O}$, $\text{Mg}(\text{NO}_3)_2 \cdot 6\text{H}_2\text{O}$, and $\text{Al}(\text{NO}_3)_3 \cdot 9\text{H}_2\text{O}$ salts with the same $\text{Cu}^{2+}/\text{Mg}^{2+}/\text{Al}^{3+}$ molar ratio as CZA-C were dissolved in 200 mL of deionized water. NaOH and Na_2CO_3 were dissolved in 350 mL of deionized water to form a mixed-base solution. Solutions A and B were added together at the same time, maintaining pH = 10.5. The resulting blue suspension was aged at 313 K for 8 h and washed by filtration several times with deionized water until the pH of filtrate reached 7.0, and the filter cake was finally dried at 393 K for 12 h. CMA-A was obtained after being calcined at the same temperature of 693 K for 4 h.

$\text{Cu}/\text{ZnO}/\text{Al}_2\text{O}_3$ catalysts (CZA-C) are commercial catalysts that are proposed to be employed in CHA hydrogenation and were provided by Catalyst Co., Ltd., SINOPEC, using a traditional co-precipitation method.

3.2. Catalyst Characterization

With an Empyrean X-ray diffractometer, samples' power X-ray diffraction (XRD) patterns were recorded using filtered CuK radiation at tube currents of 40 mA and voltages of 40 kV. All of the samples were collected between the ages of 10 and 80. Interplanar spacing and the lattice parameter were calculated by the Sheller formula.

X-ray fluorescence (XRF) on Rigaku ZSX100E was adopted to measure the contents of CuO , MgO , ZnO , and Al_2O_3 .

On a Micromeritics AutoChem 2920, the temperature-programmed reduction in hydrogen (H_2 -TPR) was determined. For H_2 -TPR, about 200 mg of each sample was pre-treated at 323 K for 1 h under argon flow (40 mL/min). The samples were then chilled to ambient temperature and heated up to 773 K using pulses of a 10% H_2/Ar gas combination at a constant rate of 283 K/min.

The Brunauer–Emmett–Teller (BET) method was used to calculate the S_{BET} surface areas from the desorption data in the relative pressure (P/P_0) range from 0.0 to 1.0. The contributions from micro- and meso-porosity were derived from the t-plot and the Barrett–Joyner–Halenda (BJH) model [47].

Surface metal contents of different copper valence states of the reduced samples were obtained from Cu 2p and Auger signal; Cu LMM was registered in the X-ray photoelectron spectroscopy (XPS) [40,41,48]. Approximately 1000 mg of the calcined catalyst was weighed and reduced in a tube furnace for 96 min after purging with nitrogen (50 mL/min) and then reducing with 10% H_2/N_2 at 453–593 K, respectively. After reduction, the catalyst was purged with nitrogen and then immediately transferred to an ethanol solution to prevent oxidation by air. Then, X-ray photoelectron spectroscopy (XPS) experiments were performed on a Thermo Fisher ESCALAB 250 spectrometer using a 150 W monochromatic Al K_{α} source to provide quantitative and chemical-state information of the sample's surface.

The pass energy of the narrow scan was set to 30 eV to obtain high-resolution spectra. The adventitious carbon located at 284.8 eV was used to calibrate samples without the carbon in themselves.

The chemical states of Cu species were obtained from Fourier transform infrared (FTIR) spectroscopy using CO as the probe molecule in vacuum cells for desorption [41,48,49]. The flake of a catalyst sample was reduced at 453–573 K, and then CO was adsorbed under liquid-nitrogen for measurements of FTIR spectra. In this work, an effective characterization method was adopted. After pressing the tablets, the reduction was first performed at 453 K, then at liquid nitrogen's temperature for CO adsorption and CO-FTIR measurements; then, the same flake was heated to 493 K for reduction, then lowered to liquid nitrogen's temperature for in situ FTIR of CO-adsorbed measurements; the reduction temperature was gradually increased, and a total of five reductions were performed until the reduction temperature reached 593 K.

The copper dispersions of the samples were measured by H₂-N₂O titration experiments on a Micromeritics Auto II 2920 apparatus with a TCD. The steps are as follows: (1) Samples were reduced in a 10% H₂-90% Ar atmosphere according to the reduction conditions, and the area of hydrogen consumption is denoted as A₁. (2) The surface copper atoms were oxidized to Cu₂O by N₂O. (3) The surface Cu₂O was reduced to copper by a 10% H₂-90% Ar atmosphere, and the area of hydrogen consumption is denoted as A₂. The dispersion (D) of copper was calculated by

$$D = (2 \times A_2 / A_1) \times 100\% \quad (1)$$

X-ray element distribution mappings and high-angle annular-dark-field (HAADF) scanning transmission electron micrographs (STEM) were obtained using a JEM ARM200F transmission electron microscope operating at 200 keV. With a probe spherical-aberration corrector, the microscope's achievable spatial resolution was 80 pm. To guarantee a suitable signal-to-noise ratio, the dwell period for image acquisition was chosen to be 40 μs per pixel.

3.3. Activity Test

The CHA hydrogenation reaction was carried out in a fixed-bed, stainless-steel reactor with an inner diameter of 14 mm. In a typical run, 15 mL of the catalyst (~10 g, 20–40 mesh) was loaded into the middle of the reactor. Before exposure to feed gas, the catalysts were reduced in a blended 10% H₂/N₂ atmosphere at 453–593 K for 16 h, respectively, which kept the reduction conditions comparable to the characteristic conditions. Then, the catalyst bed was cooled to the reaction temperature, and pure H₂ was introduced into the reactor. The feed CHA was introduced into the reactor by an SSI-III-type plunger pump, and the flow rate was controlled. The effluent from the reactor was analyzed by a gas chromatograph (Agilent 7890, with an HP-5 column), which was equipped with an FID. Four samples were taken under each reaction condition every 6–8 h to ensure reproducibility. For a thermal stability test, the catalysts were evaluated at 473 K, and then the reaction temperature was kept at 553 K for 24 h. The reaction was restarted at 473 K to compare the catalytic activity of fresh and spent catalysts. In addition to the target product, CHOL, and ethanol, the determined by-products comprised ethyl acetate, cyclohexene, cyclohexane, and cyclohexanone. Meanwhile, the conversion to CHA and the selectivity for CHOL and ethanol were calculated by

$$\text{Conv.}_{\text{CHA}} = [1 - \text{Molar amount feed after reaction} / \text{Total molar amount of feed}] \times 100\% \quad (2)$$

$$\text{Select.}_{\text{CHOL}} = \text{Molar amount of one product} / \text{Total molar amount of feed converted} \times 100\% \quad (3)$$

The initial turnover frequency (TOF) of CHA to CHOL was measured at a low CHA conversion rate. The TOF value indicates the moles of CHA converted per hour by per mole metallic copper on the catalyst's surface, which was calculated according to the following equation:

$$\text{TOF (h}^{-1}\text{)} = \frac{\text{Molar amount of CHA converted}}{\text{Molar amount of surface metallic copper on catalyst surface} \times \text{reaction time}} \quad (4)$$

The TOF value was calculated by Cu dispersion when the conversion was kept under 30%. STY represents the space–time yield of CHA for the fresh or spent catalyst, as grams of product per gram of catalyst per hour ($\text{g g}_{\text{catal}}^{-1} \text{h}^{-1}$). Data were collected after being on-stream for 6 h.

4. Conclusions

A facile co-precipitation approach was developed to prepare Cu-based precursors with the characteristics of LDH to achieve enhanced thermal stability performance in the hydrogenation from CHA to CHOL. The Cu/MgO/Al₂O₃ catalyst with an LDH precursor achieved almost excellent catalytic performance and superior stability at a lower H₂ partial pressure of 2.5 MPa (conversion, 99.59%, and selectivity, 98.94%) compared with the commercial Cu/ZnO/Al₂O₃ catalyst and amorphous Cu/MgO/Al₂O₃ catalysts. Meanwhile, higher thermal stability was observed when CMA-L was evaluated on a fixed-bed reactor after thermal treatment. Highly dispersed Cu species were much better preserved on CMA-L within the spatial confinement structure, as confirmed by STEM mapping. The relatively high thermal stability of the CMA-L catalyst was attributed to the micro-structure derived from the precursors with relatively regular structures, such as LDH, which either enhanced the interaction between Cu⁰ and Cu⁺ or inhibited the Cu species from becoming over-reduced, leaving appropriate proportions of Cu⁰ and Cu⁺. The synergistic effect of Cu⁰ and Cu⁺ species was evidenced by a reduction strategy with Cu LMM and the novel in situ FTIR of the adsorbed CO method (low-temperature liquid nitrogen conditions). The optimal performance of the CHA hydrogenation (95–97% conversion and 93–95% selectivity) was observed within a range obtained by coincidence under the reduction temperature ranges of 533 to 553 K when the Cu⁰/(Cu⁰ + Cu⁺) was near 0.70. Furthermore, the curve corresponding to the variation in Cu⁰/(Cu⁰ + Cu⁺) remained flat with the increase in reduction temperature from 533 to 553 K, which was different from previous work, in which the Cu⁰/(Cu⁰ + Cu⁺) value increased monotonously. It was proposed that the preserved micro-structure in the catalyst enhanced the interaction between Cu species and the oxide lattices, hindering in-depth CuO reduction at temperatures below 553 K. However, there are still gaps in our understanding of the formation and preservation of the above-mentioned microstructures from the precursors; the interactions between Cu species and the oxide lattices, which prevent copper from migrating and aggregating into large clusters; and the profound effects on CuO reduction. The conversion and selectivity remained up to 97% for 500 h under optimal reaction conditions. Therefore, the CMA-L catalyst with spatial constriction structures has potential commercial applications in the novel cyclohexene esterification–hydrogenation process due to its enhanced hydrogenation activity and thermal stability.

Author Contributions: Conceptualization, E.X., X.Z. and B.Z.; methodology, X.Y., L.G., H.Y. and B.Z.; formal analysis, X.Y., L.G., M.X., H.Y., A.Z., X.Z. and C.Z.; investigation, X.Y., L.G., H.Y. and B.Z.; resources, B.Z.; data curation, L.G. and E.X.; writing—original draft preparation, X.Y., L.G. and E.X.; writing—review and editing, E.X. and X.Z.; supervision, B.Z.; project administration, B.Z. All authors have read and agreed to the published version of the manuscript.

Funding: This research was funded by National Natural Science Foundation of China, grant number U19B6002.

Data Availability Statement: The research data will be made available directly from the authors upon request.

Conflicts of Interest: The authors declare no conflict of interest.

References

1. Nagaraja, B.M.; Siva Kumar, V.; Shashikala, V.; Padmasri, A.H.; Sreevardhan Reddy, S.; David Raju, B.; Rama Rao, K.S. Effect of method of preparation of copper—Magnesium oxide catalyst on the dehydrogenation of cyclohexanol. *J. Mol. Catal. A Chem.* **2004**, *223*, 339–345. [[CrossRef](#)]
2. Høiset, S.; Hjertager, B.H.; Solberg, T.; Malo, K.A. Flixborough revisited—An explosion simulation approach. *J. Hazard. Mater.* **2000**, *77*, 1–9. [[CrossRef](#)]
3. Ishida, H. Liquid-phase hydration process of cyclohexene with zeolites. *Catal. Surv. Asia* **1997**, *1*, 241–246. [[CrossRef](#)]
4. Meng, F.; Wang, Y.; Wang, S.; Wang, S. Hydration of cyclohexene over zeolite ZSM-5: Improved catalyst performance by alkali treatment. *React. Kinet. Mech. Catal.* **2016**, *119*, 671–683. [[CrossRef](#)]
5. Steyer, F.; Freund, H.; Sundmacher, K. A novel reactive distillation process for the indirect hydration of cyclohexene to cyclohexanol using a reactive entrainer. *Ind. Eng. Chem. Res.* **2008**, *47*, 9581–9587. [[CrossRef](#)]
6. Liu, H.; Jiang, T.; Han, B.; Liang, S.; Zhou, Y. Selective phenol hydrogenation to cyclohexanone over a dual supported Pd–Lewis acid catalyst. *Science* **2009**, *326*, 1250–1252. [[CrossRef](#)]
7. Zhu, Y.; Gao, L.; Wen, L.; Zong, B.; Wang, H.; Qiao, M. Cyclohexene esterification–hydrogenation for efficient production of cyclohexanol. *Green Chem.* **2021**, *23*, 1185–1192. [[CrossRef](#)]
8. Wang, Y.; Shen, Y.; Zhao, Y.; Lv, J.; Wang, S.; Ma, X. Insight into the Balancing Effect of Active Cu Species for Hydrogenation of Carbon–Oxygen Bonds. *ACS Catal.* **2015**, *5*, 6200–6208. [[CrossRef](#)]
9. Zheng, J.; Huang, L.; Cui, C.-H.; Chen, Z.-C.; Liu, X.-F.; Duan, X.; Cao, X.-Y.; Yang, T.-Z.; Zhu, H.; Shi, K.; et al. Ambient-pressure synthesis of ethylene glycol catalyzed by C₆₀-buffered Cu/SiO₂. *Science* **2022**, *376*, 288–292. [[CrossRef](#)] [[PubMed](#)]
10. Song, Y.; Zhang, J.; Lv, J.; Zhao, Y.; Ma, X. Hydrogenation of dimethyl oxalate over copper-based catalysts: Acid–base properties and reaction paths. *Ind. Eng. Chem. Res.* **2015**, *54*, 9699–9707. [[CrossRef](#)]
11. Li, Z.; Li, Y.; Wang, X.; Tan, Y.; Yang, W.; Zhu, H.; Chen, X.; Lu, W.; Ding, Y. Hydrogenation of dimethyl oxalate to ethanol over Mo-doped Cu/SiO₂ catalyst. *Chem. Eng. J.* **2023**, *454*, 140001. [[CrossRef](#)]
12. Ye, R.; Zhang, C.; Zhang, P.; Lin, L.; Huang, L.; Huang, Y.; Li, T.; Zhou, Z.; Zhang, R.; Feng, G.; et al. Facile preparation of efficient Cu-SiO₂ catalysts using a polyhydroxy molecular template to regulate surface copper species for dimethyl oxalate hydrogenation. *Catal. Commun.* **2023**, *174*, 106586. [[CrossRef](#)]
13. Bjelić, A.; Grilc, M.; Huš, M.; Likozar, B. Hydrogenation and hydrodeoxygenation of aromatic lignin monomers over Cu/C, Ni/C, Pd/C, Pt/C, Rh/C and Ru/C catalysts: Mechanisms, reaction micro-kinetic modelling and quantitative structure–activity relationships. *Chem. Eng. J.* **2019**, *359*, 305–320. [[CrossRef](#)]
14. Bjelić, A.; Grilc, M.; Likozar, B. Bifunctional metallic–acidic mechanisms of hydrodeoxygenation of eugenol as lignin model compound over supported Cu, Ni, Pd, Pt, Rh and Ru catalyst materials. *Chem. Eng. J.* **2020**, *394*, 124914. [[CrossRef](#)]
15. Bjelić, A.; Likozar, B.; Grilc, M. Scaling of lignin monomer hydrogenation, hydrodeoxygenation and hydrocracking reaction micro-kinetics over solid metal/acid catalysts to aromatic oligomers. *Chem. Eng. J.* **2020**, *399*, 125712. [[CrossRef](#)]
16. Van Den Berg, R.; Parmentier, T.E.; Elkjær, C.F.; Gommès, C.J.; Sehested, J.; Helveg, S.; De Jongh, P.E.; De Jong, K.P. Support functionalization to retard ostwald ripening in copper methanol synthesis catalysts. *ACS Catal.* **2015**, *5*, 4439–4448. [[CrossRef](#)]
17. Sun, J.; Yu, J.; Ma, Q.; Meng, F.; Wei, X.; Sun, Y.; Tsubaki, N. Freezing copper as a noble metal–like catalyst for preliminary hydrogenation. *Sci. Adv.* **2018**, *4*, eaau3275. [[CrossRef](#)] [[PubMed](#)]
18. Yu, J.; Yang, M.; Zhang, J.; Ge, Q.; Zimina, A.; Pruessmann, T.; Zheng, L.; Grunwaldt, J.-D.; Sun, J. Stabilizing Cu⁺ in Cu/SiO₂ catalysts with a shattuckite-like structure boosts CO₂ hydrogenation into methanol. *ACS Catal.* **2020**, *10*, 14694–14706. [[CrossRef](#)]
19. Zhang, Z.; Yu, J.; Zhang, J.; Ge, Q.; Xu, H.; Dallmann, F.; Dittmeyer, R.; Sun, J. Tailored metastable Ce–Zr oxides with highly distorted lattice oxygen for accelerating redox cycles. *Chem. Sci.* **2018**, *9*, 3386–3394. [[CrossRef](#)]
20. Chinchin, G.C.; Denny, P.J.; Parker, D.G.; Spencer, M.S.; Whan, D.A. Mechanism of methanol synthesis from CO₂/CO/H₂ mixtures over copper/zinc oxide/alumina catalysts: Use of ¹⁴C-labelled reactants. *Appl. Catal.* **1987**, *30*, 333–338. [[CrossRef](#)]
21. Amann, P.; Klötzer, B.; Degerman, D.; Köpfle, N.; Götsch, T.; Lömker, P.; Rameshan, C.; Ploner, K.; Bikaljevic, D.; Wang, H.-Y.; et al. The state of zinc in methanol synthesis over a Zn/ZnO/Cu(211) model catalyst. *Science* **2022**, *376*, 603–608. [[CrossRef](#)] [[PubMed](#)]
22. Behrens, M.; Studt, F.; Kasatkin, I.; Kühl, S.; Hävecker, M.; Abild-Pedersen, F.; Zander, S.; Girsdiess, F.; Kurr, P.; Kniep, B.-L.; et al. The active site of methanol synthesis over Cu/ZnO/Al₂O₃ industrial catalysts. *Science* **2012**, *336*, 893–897. [[CrossRef](#)]
23. Kattel, S.; Ramírez, P.J.; Chen, J.G.; Rodriguez, J.A.; Liu, P. Active sites for CO₂ hydrogenation to methanol on Cu/ZnO catalysts. *Science* **2017**, *355*, 1296–1299. [[CrossRef](#)] [[PubMed](#)]
24. Klier, K. Methanol Synthesis. In *Advances in Catalysis*; Eley, D.D., Pines, H., Weisz, P.B., Eds.; Academic Press: Berlin, Germany, 1982; Volume 31, pp. 243–313.
25. Kuld, S.; Thorhauge, M.; Falsig, H.; Elkjær, C.F.; Helveg, S.; Chorkendorff, I.; Sehested, J. Quantifying the promotion of Cu catalysts by ZnO for methanol synthesis. *Science* **2016**, *352*, 969–974. [[CrossRef](#)]
26. Pandit, L.; Boubnov, A.; Behrendt, G.; Mockenhaupt, B.; Chowdhury, C.; Jelic, J.; Hansen, A.-L.; Saraçi, E.; Ras, E.-J.; Behrens, M.; et al. Unravelling the Zn–Cu interaction during activation of a Zn-promoted Cu/MgO model methanol catalyst. *ChemCatChem* **2021**, *13*, 4120–4132. [[CrossRef](#)]
27. Van Den Berg, R.; Prieto, G.; Korpershoek, G.; van der Wal, L.I.; van Bunningen, A.J.; Lægsgaard-Jørgensen, S.; De Jongh, P.E.; De Jong, K.P. Structure sensitivity of Cu and CuZn catalysts relevant to industrial methanol synthesis. *Nat. Commun.* **2016**, *7*, 13057. [[CrossRef](#)]

28. Song, T.; Chen, W.; Qi, Y.; Lu, J.; Wu, P.; Li, X. Efficient synthesis of methanol and ethylene glycol via the hydrogenation of CO₂-derived ethylene carbonate on Cu/SiO₂ catalysts with balanced Cu⁺–Cu⁰ sites. *Catal. Sci. Technol.* **2020**, *10*, 5149–5162. [[CrossRef](#)]
29. Wen, C.; Cui, Y.; Dai, W.-L.; Xie, S.; Fan, K. Solvent feedstock effect: The insights into the deactivation mechanism of Cu/SiO₂ catalysts for hydrogenation of dimethyl oxalate to ethylene glycol. *Chem. Commun.* **2013**, *49*, 5195–5197. [[CrossRef](#)] [[PubMed](#)]
30. Yin, A.; Guo, X.; Dai, W.-L.; Fan, K. The Nature of Active Copper Species in Cu-HMS Catalyst for Hydrogenation of Dimethyl Oxalate to Ethylene Glycol: New Insights on the Synergetic Effect between Cu⁰ and Cu⁺. *J. Phys. Chem. C* **2009**, *113*, 11003–11013. [[CrossRef](#)]
31. Zheng, X.; Lin, H.; Zheng, J.; Duan, X.; Yuan, Y. Lanthanum oxide-modified Cu/SiO₂ as a high-performance catalyst for chemoselective hydrogenation of dimethyl oxalate to ethylene glycol. *ACS Catal.* **2013**, *3*, 2738–2749. [[CrossRef](#)]
32. Xia, S.; Nie, R.; Lu, X.; Wang, L.; Chen, P.; Hou, Z. Hydrogenolysis of glycerol over Cu_{0.4}/Zn_{5.6-x}Mg_xAl₂O_{8.6} catalysts: The role of basicity and hydrogen spillover. *J. Catal.* **2012**, *296*, 1–11. [[CrossRef](#)]
33. Zhang, S.; Fan, G.; Li, F. Lewis-base-promoted copper-based catalyst for highly efficient hydrogenation of dimethyl 1,4-cyclohexane dicarboxylate. *Green Chem.* **2013**, *15*, 2389–2393. [[CrossRef](#)]
34. Qi, Y.; Song, T.; Li, K.; Wu, P.; Zhu, Z.; Li, X. Synthesis of cyclohexanol and ethanol via the hydrogenation of cyclohexyl acetate with Cu₂Zn_x/Al₂O₃ catalysts. *Catal. Sci. Technol.* **2021**, *11*, 7035–7046. [[CrossRef](#)]
35. Shi, J.; He, Y.; Ma, K.; Tang, S.; Liu, C.; Yue, H.; Liang, B. Cu active sites confined in MgAl layered double hydroxide for hydrogenation of dimethyl oxalate to ethanol. *Catal. Today* **2021**, *365*, 318–326. [[CrossRef](#)]
36. Ren, Y.; Yang, Y.; Chen, L.; Wang, L.; Shi, Y.; Yin, P.; Wang, W.; Shao, M.; Zhang, X.; Wei, M. Synergetic effect of Cu⁰–Cu⁺ derived from layered double hydroxides toward catalytic transfer hydrogenation reaction. *Appl. Catal. B Environ.* **2022**, *314*, 121515. [[CrossRef](#)]
37. Schwenk, C.F.; Rode, B.M. The influence of the Jahn–Teller effect and of heteroligands on the reactivity of Cu²⁺. *Chem. Commun.* **2003**, *11*, 1286–1287. [[CrossRef](#)]
38. Gong, J.; Yue, H.; Zhao, Y.; Zhao, S.; Zhao, L.; Lv, J.; Wang, S.; Ma, X. Synthesis of Ethanol via Syngas on Cu/SiO₂ Catalysts with Balanced Cu⁰–Cu⁺ Sites. *J. Am. Chem. Soc.* **2012**, *134*, 13922–13925. [[CrossRef](#)]
39. Yao, Y.; Wu, X.; Gutiérrez, O.Y.; Ji, J.; Jin, P.; Wang, S.; Xu, Y.; Zhao, Y.; Wang, S.; Ma, X.; et al. Roles of Cu⁺ and Cu⁰ sites in liquid-phase hydrogenation of esters on core-shell CuZn_x@C catalysts. *Appl. Catal. B Environ.* **2020**, *267*, 118698. [[CrossRef](#)]
40. Dai, W.-L.; Sun, Q.; Deng, J.-F.; Wu, D.; Sun, Y.-H. XPS studies of Cu/ZnO/Al₂O₃ ultra-fine catalysts derived by a novel gel oxalate co-precipitation for methanol synthesis by CO₂ + H₂. *Appl. Surf. Sci.* **2001**, *177*, 172–179. [[CrossRef](#)]
41. Hu, J.; Li, Y.; Zhen, Y.; Chen, M.; Wan, H. In situ FTIR and ex situ XPS/HS-LEIS study of supported Cu/Al₂O₃ and Cu/ZnO catalysts for CO₂ hydrogenation. *Chin. J. Catal.* **2021**, *42*, 367–375. [[CrossRef](#)]
42. Li, D.; Xu, F.; Tang, X.; Dai, S.; Pu, T.; Liu, X.; Tian, P.; Xuan, F.; Xu, Z.; Wachs, I.E.; et al. Induced activation of the commercial Cu/ZnO/Al₂O₃ catalyst for the steam reforming of methanol. *Nat. Catal.* **2022**, *5*, 99–108. [[CrossRef](#)]
43. Cui, G.; Meng, X.; Zhang, X.; Wang, W.; Xu, S.; Ye, Y.; Tang, K.; Wang, W.; Zhu, J.; Wei, M.; et al. Low-temperature hydrogenation of dimethyl oxalate to ethylene glycol via ternary synergistic catalysis of Cu and acid–base sites. *Appl. Catal. B Environ.* **2019**, *248*, 394–404. [[CrossRef](#)]
44. Gong, X.; Wang, M.; Fang, H.; Qian, X.; Ye, L.; Duan, X.; Yuan, Y. Copper nanoparticles socketed in situ into copper phyllosilicate nanotubes with enhanced performance for chemoselective hydrogenation of esters. *Chem. Commun.* **2017**, *53*, 6933–6936. [[CrossRef](#)]
45. Dandekar, A.; Vannice, M.A. Determination of the Dispersion and Surface Oxidation States of Supported Cu Catalysts. *J. Catal.* **1998**, *178*, 621–639. [[CrossRef](#)]
46. Sakakini, B.; Tabatabaei, J.; Watson, M.J.; Waugh, K.C. Structural changes of the Cu surface of a Cu/ZnO/Al₂O₃ catalyst, resulting from oxidation and reduction, probed by CO infrared spectroscopy. *J. Mol. Catal. A-Chem.* **2000**, *162*, 297–306. [[CrossRef](#)]
47. Lv, M.; Liu, H. Photocatalytic property and structural stability of CuAl-based layered double hydroxides. *J. Solid State Chem.* **2015**, *227*, 232–238. [[CrossRef](#)]
48. Chen, Y.; Hong, H.; Cai, J.; Li, Z. Highly Efficient CO₂ to CO Transformation over Cu-Based Catalyst Derived from a CuMgAl-Layered Double Hydroxide (LDH). *ChemCatChem* **2021**, *13*, 656–663. [[CrossRef](#)]
49. Batyrev, E.D.; van den Heuvel, J.C.; Beckers, J.; Jansen, W.P.A.; Castricum, H.L. The effect of the reduction temperature on the structure of Cu/ZnO/SiO₂ catalysts for methanol synthesis. *J. Catal.* **2005**, *229*, 136–143. [[CrossRef](#)]

Disclaimer/Publisher’s Note: The statements, opinions and data contained in all publications are solely those of the individual author(s) and contributor(s) and not of MDPI and/or the editor(s). MDPI and/or the editor(s) disclaim responsibility for any injury to people or property resulting from any ideas, methods, instructions or products referred to in the content.